Available online at www.sciencedirect.com
ScienceDirect
Catalysis Today 120 (2007) 270–275
CATALYSIS TODAY
www.elsevier.com/locate/cattod

Hydrogen sorption of magnesium hydride doped with nano-sized TiO_2

Kyung Sub Jung *, Dong Hyun Kim, Eun Young Lee, Kyung Sub Lee

Division of Advanced Materials and Science and Engineering, Hanyang University, Seoul 133-791, Republic of Korea

Available online 8 December 2006

Abstract

Various phases of TiO_2 such as anatase, rutile and commercial P25 were added to magnesium hydride by high-energy ball milling in order to improve the hydriding properties of the magnesium. After 1 h milling, the sample containing nano-size rutile powder (200–400 nm) showed uniform distribution, while other shapes of TiO_2 added samples did in separate phase. The effect of the rutile concentrations (3, 5, 7 and 10 mol%) on the hydrogen sorption property of MgH_2 has been investigated and found that the sample containing 5 mol% rutile had the highest hydrogen capacity of 4.40 wt.% at 300 °C and 3.54 wt.% at 250 °C. This amount of hydrogen absorption is still lower than the pure magnesium requires a long activation time, however, its kinetics of hydrogen sorption was greatly enhanced. Moreover, hydrogen absorption capacity was slightly increased with the increase in number of cycles. The mechanism of catalytic effect of uniformly distributed TiO_2 and TiO_2 dispersed as discrete particles in magnesium matrix has been discussed based on microstructural observations.

Keywords: Magnesium hydride; Oxide catalysis; Hydrogen absorption; Rutile TiO_2

1. Introduction

A key technical challenge in fuel cell powered on-boarding vehicles is the development of an effective hydrogen storage system. There have been many attempts to develop hydrogen storage materials that can meet the effective capacity, reaction temperature, operating pressure and safety requirements at a reasonable cost [1]. Among the variable hydrogen storage systems, metal hydrides are one of the most promising candidates of the stable hydrogen storage materials. So far, many metal hydrides have been developed for practical use such as $LaNi_5$ and TiFe. However, the stored hydrogen weight percentages for these materials are too low for practical storage of hydrogen. Therefore, there is a need to create hydrides based on light metals [2].

Magnesium and magnesium-based hydrogen storage materials are among the most promising materials for such a system. Magnesium has a large theoretical hydrogen storage capacity (7.6 wt.%), low cost and it is lighter than other metal hydride [3]. However, the hydriding and dehydriding reactions occur only at a high temperature and high pressure with low kinetics [4,5]. Researchers have tried to overcome these problems by manufacturing nanocrystalline magnesium powder [6–10], synthesizing composite metal hydride [14–19] and adding catalysts [20–23].

There are several advantages to manufacturing nanocrystalline powder by high-energy ball milling. The nanocrystalline hydrides synthesized by high-energy ball milling showed very fast absorption and desorption kinetics due to faster diffusion of hydrogen along grain boundaries, as well as the high number of heterogeneous nucleation sites of the hydride on absorption [11]. The ball milling process reduces the size of magnesium hydride particles and increases effective surface reaction areas of the magnesium–hydrogen interfaces and induces stresses and defects in the structure which can enhance the hydrogen diffusion [24,25]. Composite hydrides have relatively high capacity, favorable thermodynamics and kinetics in hydriding/dehydriding process. Recently, the effect of transition metals (Ti, V, Mn, Fe and Ni) on magnesium has been investigated by Liang et al. [12–15]. They showed that ball-milled MgH_2 with addition of 5 at.% of a transition metal absorbed hydrogen at room temperature (1 MPa) and desorbed at 235 °C (0.015 MPa).

Oelerich et al. [21] used metal oxides as a catalyst for improving the kinetics of hydrogen absorption of magnesium based materials fabricated by high-energy ball milling. It was found that the transition-metal oxides such as TiO_2, V_2O_5,

* Corresponding author. Tel.: +82 2 2281 4914; fax: +82 2 2281 4914.
E-mail address: skjskj98@paran.com (K.S. Jung).

0920-5861/$ – see front matter © 2006 Elsevier B.V. All rights reserved.
doi:10.1016/j.cattod.2006.09.028

Cr_2O_3, Mn_2O_3 and Fe_3O_4 acted as catalysts for the magnesium–hydrogen reaction. However, time for the manufacture of nanocrystalline magnesium powder, synthesis of composite hydride and addition of catalysts are time consuming processes.

Schober [26] reported that dissolving hydrogen by TiO_2 after dissociation of hydrogen molecules could provide an effective path for hydrogen penetration of TiFe–TiO_2 composite systems. This study showed that TiO_2 had the highest potential as a catalyst for improving the hydrogen sorption properties of metal hydride. In spite of many researches carried out on the Mg–TiO_2 system, it is hard to satisfy the capacity requirement of hydrogen storage system.

The aim of this study is to investigate the hydrogenation properties of MgH_2 with the various types of nano-sized TiO_2 (rutile, anatase and commercial P25) by high-energy ball milling to improve the hydrogen storage capacity and kinetics of hydriding of Mg.

2. Experimental

Five-mole percentage of various TiO_2 phases (rutile, anatase and commercial P25) with β-MgH_2, and rutile TiO_2 (3, 5, 7 and 10 mol%) with β-MgH_2 were charged in a Cr–Ni steel vial together with two 1/2 in. and four 1/4 in. diameter steel balls. The physical characterizations of the starting material are listed in Table 1. The samples were ball-milled using a SPEX 8000 miller for 1 h, with a ball-to-powder ratio of 10:1. All the processes for manufacturing powders were done in argon filled glove box to prevent oxidation of the samples.

Phase of the samples was characterized by X-ray diffraction (XRD: Rigaku-denki D/max 2500) using Cu Kα (λ = 1.5418 Å). Microstructure studies were performed with a transmission electron microscope (TEM: JEM-2010) equipped an energy dispersive X-ray spectrometer (EDX) and an X-ray photoelectron spectroscope (XPS).

The hydrogen absorption kinetics and cycle tests were evaluated by the conventional volumetric pressure–composition (*P–C*) isotherm method using an automated Sivert's type apparatus following the procedures described elsewhere [27]. 0.5 g of the synthesized samples were loaded into a steel reactor and hydrogen gas (purity: 99.9999%) at a pressure of 10 atm was introduced after an initial dehydriding for 20 h in a vacuum at 350 °C for hydrogen absorption kinetic testing. The kinetics of each sample was measured at 300 and 250 °C.

Table 1
Characterizations of starting materials

	Powder			
	β-MgH_2	Rutile	Anatase	Commercial P25 (70% anatase + 30% rutile)
Purity (%)	95	99.5	99.7	99.5
Size	40 μm	100–200 nm	15–50 nm	30–50 nm
Shape	Tetragonal (primitive)	Tetragonal (primitive)	Tetragonal (BCC)	Tetragonal (primitive + BCC)

3. Results and discussion

3.1. Sample characterization

Fig. 1(a) shows the XRD patterns of the ball-milled MgH_2-$(rutile)_{0.05}$, MgH_2-$(anatase)_{0.05}$ and MgH_2-$(commercial\ P25)_{0.05}$. All MgH_2 had peaks of β-phase. Characteristic peaks for rutile phase in the ball-milled samples with MgH_2 were not observed, while other types of the TiO_2 peaks were detected in XRD analysis. The uniform distribution of rutile in MgH_2 was probably due to both rutile TiO_2 and MgH_2 having a tetragonal (primitive) shape with similar lattice parameters ($a = b =$ 4.5163 Å, $c = 3.0205$ Å for MgH_2 and $a = b = 4.5172$ Å,

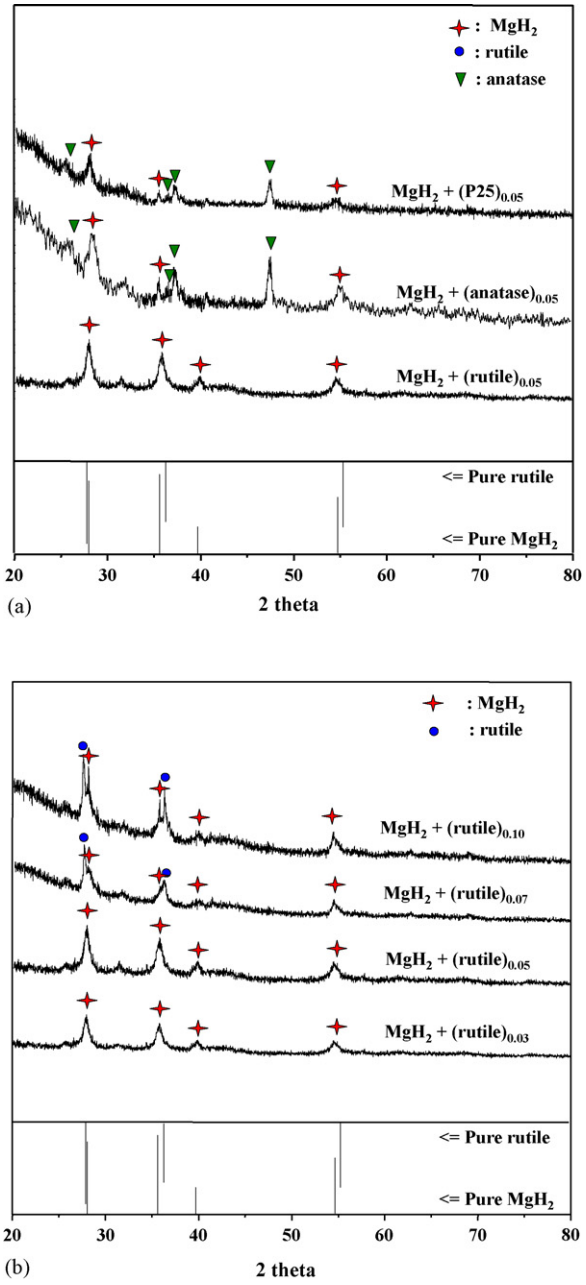

Fig. 1. (a) XRD patterns of 5 mol% added ball-milled sample and (b) XRD patterns of ball-milled sample as a function of rutile concentration.

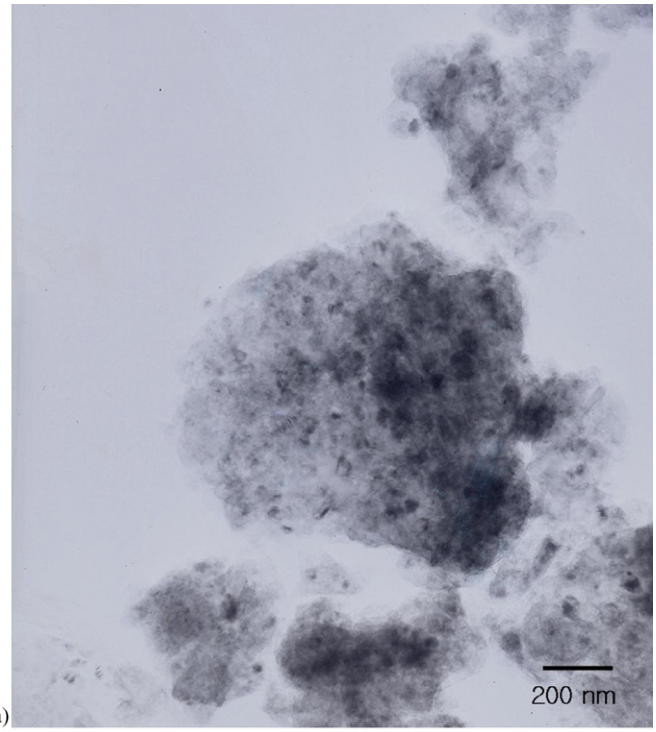

(a)

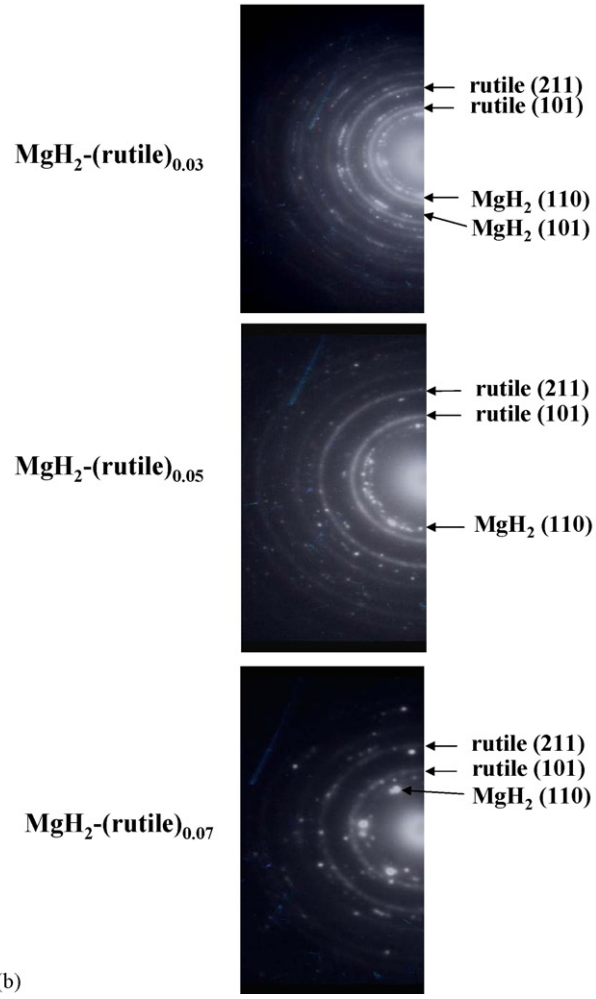

(b)

Fig. 2. (a) TEM morphology of MgH_2-(rutile)$_{0.03}$ and (b) SAD patterns of MgH_2-(rutile)$_{0.03,\ 0.05\ \text{and}\ 0.07}$.

$c = 2.943$ Å for rutile) while, anatase TiO_2 has a tetragonal (BCC) structure and much different lattice parameters ($a = b = 3.738$ Å, $c = 9.4976$ Å). The uniform distribution of rutile in MgH_2 matrix was confirmed using TEM analysis presented below. Fig. 1(b) shows the XRD patterns of MgH_2-(rutile)$_X$ as a function of rutile concentration ($X = 0.03, 0.05, 0.07$ and 0.10). It can be seen from the figure that rutile peaks are absent when its concentration was kept less than 5 mol%. However, rutile peaks are observed above 5 mol%. To further investigate for the effects of the rutile concentration on the hydrogen sorption property of MgH_2, TEM analyses were carried out to observe the morphologies and crystal structures of the samples. All MgH_2-(rutile)$_x$ samples ($x = 0.03, 0.05, 0.07$ and 0.10) has been found to show a similar morphology. Fig. 2(a) shows a representative TEM micrograph of the MgH_2-(rutile)$_{0.03}$. The sample MgH_2-(rutile)$_{0.03}$ consists of black TiO_2 and ashy MgH_2 spherical particles with an average grain size of 300 nm. SAD patterns of the samples as a function of rutile concentration are shown in Fig. 2(b). SAD patterns of MgH_2-(rutile)$_{0.03}$ show diffraction rings of nano rutile TiO_2 and diffraction spots of MgH_2 due to the relatively large grain size of MgH_2. As rutile concentration increased, spot patterns of MgH_2 became increasingly single-crystal-like whereas the intensity of rutile diffraction ring decreased, especially at $x = 0.07$. The dark field image in Fig. 3 was formed using the rutile (1 0 1) diffraction ring and shows that rutile crystallites are evenly distributed inside the MgH_2 particle. Judging from the micrograph, the average rutile particle size is from 20 to 90 nm. This morphology suggests that the MgH_2-(rutile)$_{0.05}$ nanocomposite may have been formed due to the cold welding and fracture during the ball milling. This observation also matches well with the conclusion of Wang et al. [28] who suggested that MgH_2 and rutile could form nanocomposite.

In order to further investigate the compositional distribution of the rutile, EDX was performed on MgH_2-(rutile)$_{0.07}$ and the obtained results are shown in Fig. 4. At this composition, rutile was no longer evenly distributed inside the MgH_2 grain as confirmed by EDX. EDX data in Fig. 4 show that some region was enriched with Ti while another region, in the same grain, was nearly free of Ti. It appears that MgH_2 and rutile exist as a separate phase. The most likely reason for this observation may be due to an excess of rutile (above 5 mol%). This indicates that the uniform nanocomposite could be formed by the optimum

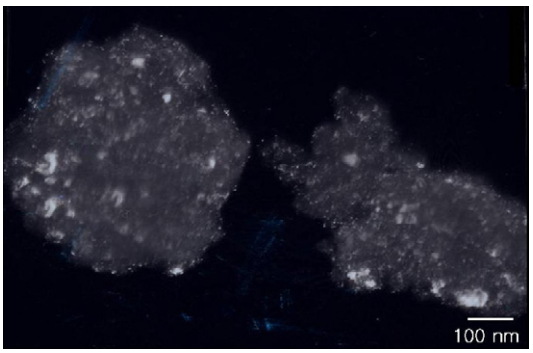

Fig. 3. Dark field image using rutile (1 0 1) ring of MgH_2-(rutile)$_{0.05}$.

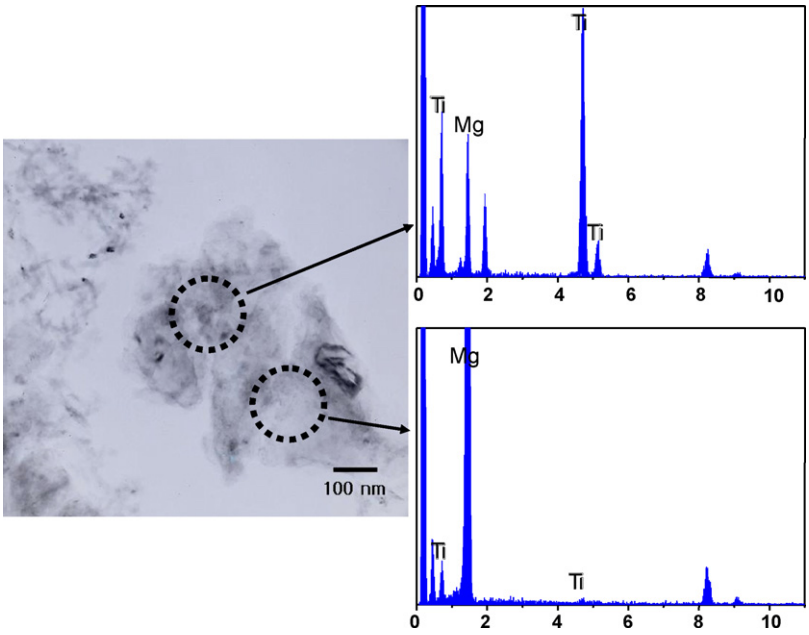

Fig. 4. EDX pattern of the MgH_2-(rutile)$_{0.07}$.

amount of rutile TiO_2 below $x = 0.05$. To obtain the chemical state of the catalytic effect of rutile on MgH_2, XPS analysis was performed. Fig. 5 shows that the Mg 2p XPS peaks. Owing to the formation of nanocomposite, both MgH_2-(rutile)$_{0.03}$ and MgH_2-(rutile)$_{0.05}$ were shifted to a high binding energy position. However, MgH_2-(rutile)$_{0.07}$ had a binding energy of both pure MgH_2 and composite, and the average peak is shown between pure MgH_2 and other compositions of rutile added samples due to the separation of MgH_2 and rutile. This result agrees well with TEM analysis.

3.2. Pressure–composition isotherm analysis

Fig. 6 shows the hydrogen absorption kinetics of MgH_2-(rutile)$_{0.05}$, MgH_2-(anatase)$_{0.05}$, MgH_2-(commercial P25)$_{0.05}$

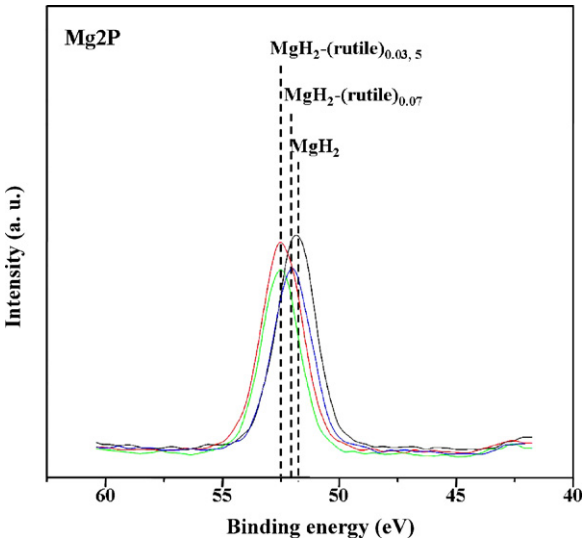

Fig. 5. XPS-photoelectron peaks of MgH_2, MgH_2-(rutile)$_{0.03}$, MgH_2-(rutile)$_{0.05}$, and MgH_2-(rutile)$_{0.07}$.

and ball-milled MgH_2 at 300 and 250 °C. Fig. 6(a) shows that the hydrogen absorption capacity of MgH_2-(rutile)$_{0.05}$ is 4.40 wt.% at 300 °C. This amount of hydrogen absorption is still lower than the theoretical capacity of pure magnesium. However, the hydrogen absorption kinetics MgH_2-(rutile)$_{0.05}$ was 10 times faster than that of ball-milled MgH_2. There was no increase in the absorption capacity and kinetics for the anatase added sample. Similar absorption capacities of about 3.56 wt.% were observed for MgH_2-(commercial P25)$_{0.05}$ and ball-milled MgH_2. However, the hydrogen absorption kinetics of P25 added sample showed higher than that of ball-milled MgH_2. Because P25 has the effects of both rutile and anatase on hydrogenation, the hydrogen absorption kinetics of P25 added sample showed lower than rutile added sample but higher than ball-milled MgH_2. Fig. 6(b) shows at 250 °C that the rutile added sample has the highest absorption capacity and the fastest kinetics. Moreover, the kinetics of hydrogen absorption of rutile added sample is about 100 times faster than that of MgH_2. The increased hydrogen absorption and capacity kinetics of the rutile added sample could be explained by the formation of nanocomposite with MgH_2. The hydrogen absorption kinetics and capacity of the sample at 300 and 250 °C are listed in Table 2. All of the hydrogen absorption kinetics was calculated from the initial hydrogen capacity to 80% of the maximum hydrogen absorption capacity using the numerical least-square method.

Fig. 7 shows the cycle test of MgH_2-(rutile)$_{0.05}$. The maximum hydrogen absorption was shown after the second cycle at both 300 and 250 °C because of the initial activation. Considering the result of absorption capacities and kinetics, only rutile exhibited a catalytic effect on MgH_2.

The hydrogen absorption kinetics was carried out as a function of the rutile concentration in order to perform a more detailed study of the catalytic effect of the rutile. TEM

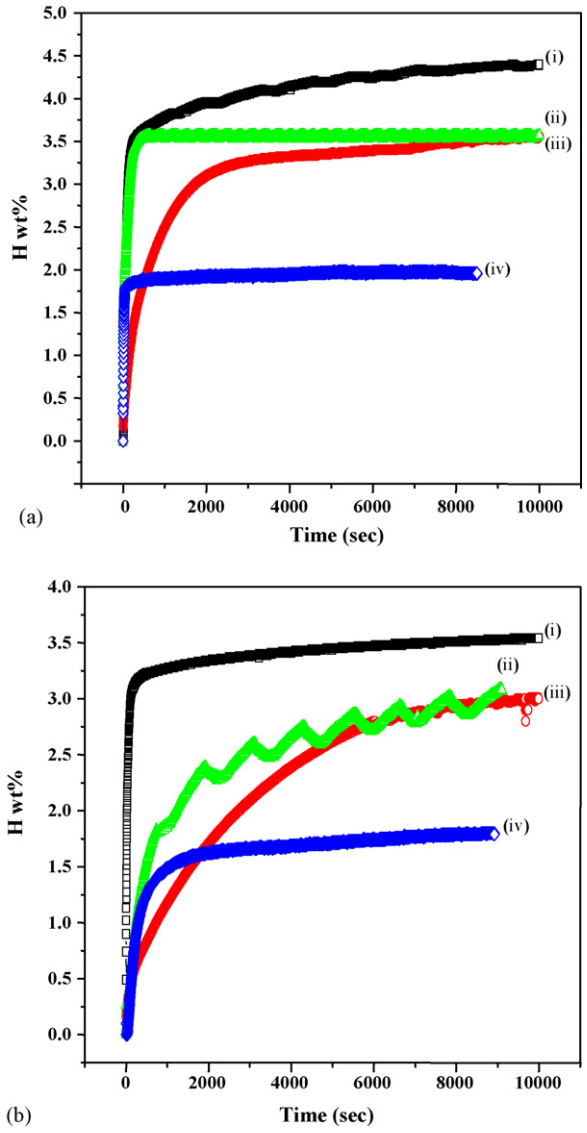

Fig. 6. (a) Hydrogen absorption kinetics of (i) MgH_2-(rutile)$_{0.05}$; (ii) MgH_2-(commercial P25)$_{0.05}$; (iii) ball-milled MgH_2; (iv)MgH_2-(anatase)$_{0.05}$ at 300 °C, 10 atm. (b) Hydrogen absorption kinetics of (i) MgH_2-(rutile)$_{0.05}$; (ii) MgH_2-(commercial P25)$_{0.05}$; (iii) ball-milled MgH_2; (iv) MgH_2-(anatase)$_{0.05}$ at 250 °C, 10 atm.

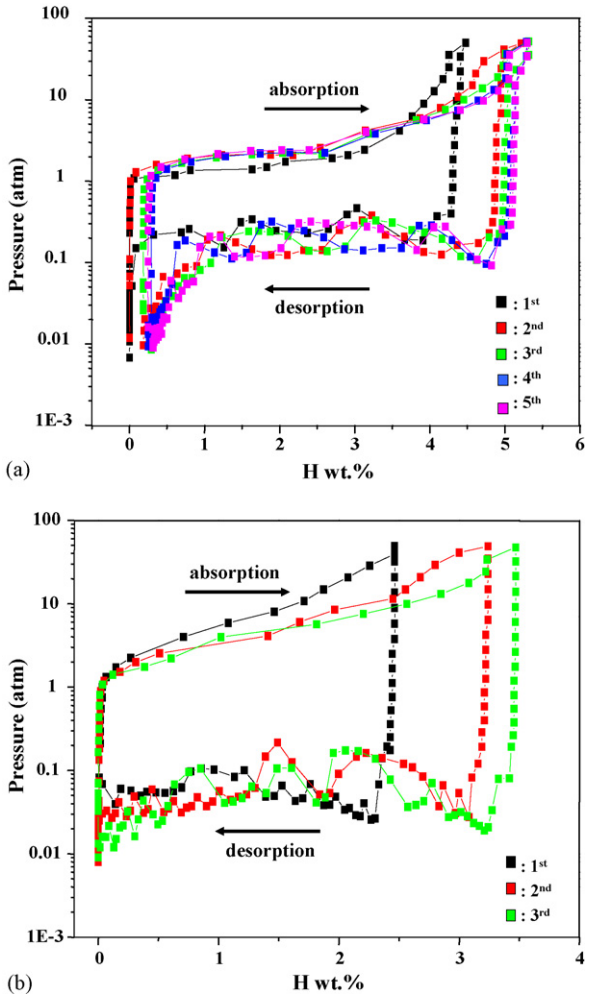

Fig. 7. (a) Cycle test of MgH_2-(rutile)$_{0.05}$ at 300 °C and (b) cycle test of MgH_2-(rutile)$_{0.05}$ at 250 °C.

and XPS analyses showed that the optimum concentration of rutile on MgH_2 was 5 mol%. This matches well with the hydrogen absorption kinetics. Fig. 8 shows that the maximum hydrogen absorption and fastest kinetics were observed for the 5 mol% rutile added sample at both 300 and 250 °C due to the uniformly distributed nanocomposites. The relatively less uniformed formation of nanocomposite on the 3 mol% added sample and the separated phase of MgH_2 and rutile on 7 mol% might have a slight catalytic effect on MgH_2.

Table 2
Hydrogen absorption kinetics and capacities of the samples at 300 and 250 °C, 10 atm

Powder	300 °C		250 °C	
	Kinetics (wt.%/s)	Hydrogen capacities (wt.%)	Kinetics (wt.%/s)	Hydrogen capacities (wt.%)
MgH_2-(rutile)$_{0.05}$	0.013	4.40	0.021	3.54
MgH_2-(P25)$_{0.05}$	0.012	3.57	0.001	3.08
Ball-milled MgH_2	0.001	3.56	0.002	3.00
MgH_2-(anatase)$_{0.05}$	0.005	1.95	0.002	1.79

A high density of nanocomposite on the sample would accelerate the hydrogenation of Mg. It is generally accepted that the most difficult step in hydrogen absorption is the diffusion of hydrogen through the pre-formed hydride. The uniform distribution of rutile on the MgH_2 surface could prevent hydrogenation on the surface layer of the Mg, which would increase the available paths for hydrogen diffusion resulting in the catalytic effect of rutile. Moreover, the use of nano-sized MgH_2-(rutile)$_{0.05}$ creates a greater reactive surface with hydrogen. Ball milling of MgH_2 and TiO_2 created a nanocomposite with an ultra fine structure.

The formation of uniformly distributed nanocomposite and ultra fine structure caused by high-energy ball milling enhanced the hydrogenation of Mg.

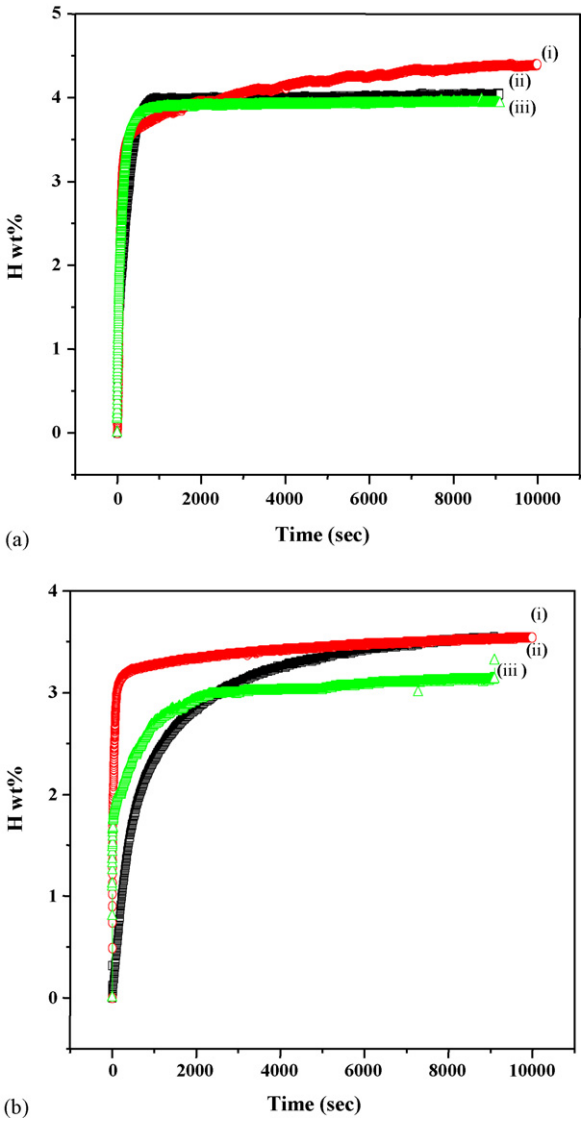

Fig. 8. (a) Hydrogen absorption kinetics of (i) MgH_2-(rutile)$_{0.05}$; (ii) MgH_2-(rutile)$_{0.03}$; (iii) MgH_2-(rutile)$_{0.07}$ at 300 °C, 10 atm. (b) Hydrogen absorption kinetics of (i) MgH_2-(rutile)$_{0.05}$; (ii) MgH_2-rutile)$_{0.03}$; (iii) MgH_2-(rutile)$_{0.07}$ at 250 °C, 10 atm.

4. Conclusions

MgH_2-(various TiO_2)$_{0.05}$ (rutile, anatase and commercial P25) and MgH_2-(rutile)$_x$ (x = 0.03, 0.05 and 0.07) synthesized by high-energy ball milling were investigated to enhance the hydrogenation properties of Mg. Among the various TiO_2 phases, rutile showed the fastest absorption kinetics and highest capacity. A rutile concentration of 5 mol% exhibited the best catalytic effect.

The hydrogen absorption kinetics and capacity were increased by forming the ultra fine nanocomposite of MgH_2-(rutile)$_{0.05}$. The results from this study show that the MgH_2-rutile nanocomoposite phase can be an effective material for hydrogen storage on a large scale.

Acknowledgements

This research (paper) was performed for the Hydrogen Energy R&D Center, one of the 21st Century Frontier R&D Programs, funded by the Ministry of Science and Technology of Korea.

The authors express their heartfelt thanks to Prof. Chong Seung Yoon for valuable discussions.

References

[1] L. Schlapbach, A. Zuttel, Nature 414 (2001) 353.
[2] T. Noritake, M. Aoki, S. Towata, Y. Seno, Y. Hirose, E. Nishibori, M. Takata, M. Sakata, Appl. Phys. Lett. 81 (2002) 2008.
[3] H. Yuan, Y. An, G. Xu, C. Chen, Mater. Chem. Phys. 83 (2004) 340.
[4] B. Vigeholm, J. Kjoller, B. Larsen, A.S. Pedersen, J. Less-Common Met. 89 (1983) 135.
[5] B. Bogdanovic, T.H. Hartwing, B. Spliethoff, Int. J. Hydrogen Energy 18 (1993) 575.
[6] J. Huot, M.L. Tremblay, R. Schulz, J. Alloys Compd. 356/357 (2003) 603.
[7] J.L. Bobet, S. Desmoulins-Krawiec, E. Grigorova, R. Cansell, B. Chevalier, J. Alloys Compd. 351 (2003) 217.
[8] L. Zaluski, A. Zaluska, P. Tessier, J.O. Strom-Olsen, R. Schulz, Mater. Sci. Forum 225 (1996) 853.
[9] L. Zaluski, A. Zaluska, P. Tessier, K.H. Ryan, J.O. Strom-Olsen, M.L. Trudeau, R. Schulz, J. Phys. Chem. 183 (1994) 45.
[10] K.J. Gross, P. Spatz, A. Zuttel, L. Schlapbach, J. Alloys Compd. 240 (1996) 206.
[11] Z. Dehouche, T. Klassen, W. Oelerich, J. Goyette, T.K. Bose, R. Schulz, J. Alloys Compd. 347 (2002) 319.
[12] G. Liang, S. Boily, J. Huot, A. Van Neste, R. Schulz, J. Alloys Compd. 267 (1998) 302.
[13] G. Liang, S. Boily, J. Huot, A. Van Neste, R. Schulz, J. Alloys Compd. 268 (1998) 302.
[14] G. Liang, J. Huot, S. Boily, A.V. Neste, R. Schulz, J. Alloys Compd. 291 (1999) 295.
[15] G. Liang, J. Huot, S. Boily, R. Schulz, J. Alloys Compd. 305 (2000) 239.
[16] S.R. Ovshinsky, M.A. Fetcenko, Appl. Phys. B 72 (2001) 239.
[17] J. Huot, J.F. Pelletier, L.B. Lurio, M. Sutton, R. Schulz, J. Alloys Compd. 248 (2003) 319.
[18] J. Huot, G. Liang, R. Schulz, J. Alloys Compd. 353 (2003) L12.
[19] G. Liang, J. Alloys Compd. 370 (2004) 123.
[20] G. Liang, J. Huot, S. Boily, A.V. Neste, R. Schulz, J. Alloys Compd. 292 (1999) 247.
[21] W. Oelerich, T. Klassen, R. Bormann, J. Alloys Compd. 315 (2001) 237.
[22] J.F. Pelletier, J. Huot, M. Sutton, R. Schulz, A.R. Sandy, L.B. Lurio, S.G.J. Mochrie, Phys. Rev. B 63 (2001) 052103.
[23] L. Zaluski, A. Zaluska, J.O. Strom-Olsen, J. Alloys Compd. 289 (1999) 197.
[24] J. Huot, G. Liang, S. Boily, A.V. Neste, R. Schulz, J. Alloys Compd. 293–295 (1999) 495.
[25] L. Zaluski, A. Zaluska, J.O. Strom-Olsen, J. Alloys Compd. 253/254 (1997) 70.
[26] T. Schober, J. Less-Common Met. 89 (1983) 63.
[27] R. Checchetto, G. Trettel, A. Miotello, Meas. Sci. Technol. 15 (2004) 127.
[28] P. Wang, A.M. Wang, H.F. Zhang, B.Z. King, Z.Q. Hu, J. Alloys Compd. 313 (2000) 218.